Biological Journal of the Linnean Society, 2018, **XX**, 1–16. With 7 figures.

Filtration area scaling and evolution in mysticetes: trophic niche partitioning and the curious cases of sei and pygmy right whales

ALEXANDER J. WERTH[1]*, JEAN POTVIN[2], ROBERT E. SHADWICK[3], MEGAN M. JENSEN[4], DAVID E. CADE[4] and JEREMY A. GOLDBOGEN[4]

[1]*Department of Biology, Hampden-Sydney College, Hampden-Sydney, VA 23943, USA*
[2]*Department of Physics, Saint Louis University, St. Louis, MO 63103, USA*
[3]*Department of Zoology, University of British Columbia, Vancouver, B.C., Canada V6T 1Z4*
[4]*Department of Biology, Hopkins Marine Station, Stanford University, Pacific Grove, CA 93950, USA*

Received 16 May 2018; revised 22 July 2018; accepted for publication 23 July 2018

We analysed the functional morphology and hydrodynamics of the filtering apparatus in ten species of baleen whales (Mysticeti). Our results demonstrate a clear demarcation in baleen scaling of continuous ram filter feeders (Balaenidae; right and bowhead whales) and intermittent lunge/suction feeders: rorquals (Balaenopteridae) and the grey whale (Eschrichtiidae). In addition to different scaling trajectories, filter area varies widely among taxa. Balaenid baleen has four to five times the area of that of similarly sized rorquals (by body length and mass). Filter areas correlate with morphology; lineages evidently evolved to exploit different types of patchy prey. Feeding performance data from hydrodynamic modelling and tagged whales suggest that drag forces limit balaenids, whereas time required to purge and filter engulfed water appears to limit rorquals. Because scaling of engulfment volume outpaces increases in baleen area, large rorquals must devote greater proportions of dive time to filtration. In contrast, balaenids extend dive duration, but as a trade-off are limited to low engulfment speeds and therefore can only target prey with low escape capabilities. The sei whale, *Balaenoptera borealis*, has a mid-range filter reflecting its transitional diet and intermediate morphology, embodying generalized characteristics of both continuous ram and intermittent lunge filtration. The pygmy right whale, *Caperea marginata*, has a balaenid-type filter via 2D analysis, but enhanced 3D modelling shows *Caperea*'s baleen fits better with rorquals. Allometric equations relating body and filter size address phylogenetic questions about filtration in extinct lineages, including future ancestor state reconstruction analyses. Based on baleen and body size (~5 m) and skull morphology, the earliest edentulous mysticetes were probably intermittent rather than continuous filterers, with simple baleen.

ADDITIONAL KEYWORDS: baleen – diet – drag – energetics – filter feeding – guild – morphology – phylogeny – whale.

INTRODUCTION

Fundamental scaling relationships that influence the function of key feeding structures play a major role in shaping the performance, ecology and evolution of organisms. Although obligate filter feeding and gigantism evolved multiple times in aquatic vertebrates, little is known about performance capabilities and ecological consequences of this innovation in the largest and most recent radiation of gigantic microphagous vertebrates: baleen whales (Mammalia: Mysticeti).

*Corresponding author. E-mail: awerth@hsc.edu

Filtration is the most efficient means of capturing small aquatic prey, especially in bulk (Lauder, 1985; Sanderson & Wassersug, 1990). Suspension filter feeding is common in marine invertebrates and evolved multiple times in vertebrates, including several lineages of gigantic cartilaginous and bony fishes. Mysticetes also evolved obligate filter feeding and consequently attained giant body size (Pyenson, 2017; Slater *et al.*, 2017; Goldbogen & Madsen, 2018). Since mysticetes evolved a sieve-like filter in place of dentition, taking advantage of Oligocene oceanographic changes approximately 30 Mya (Deméré *et al.*, 2008; Gatesy *et al.*, 2013; Marx & Fordyce, 2015; Berta *et al.*,

2016), they diversified and evolved huge bodies by feeding near the base of the trophic pyramid, thereby increasing energetic efficiency (Werth, 2000; Goldbogen *et al.*, 2011; Pyenson & Vermeij, 2016; Slater *et al.*, 2017). Despite the preponderance of gigantic marine filterers, the underlying physiological and ecological mechanisms that drove this ecomorphological evolution remain poorly understood.

Baleen is a neomorphic keratinous oral tissue with no functional analogue or evolutionary homologue. It defines crown mysticetes. The comb-like filtering apparatus comprises bilaterally paired 'racks' of 200–300 transversely orientated triangular plates that hang, suspended from palatal gingiva, like vertical blinds spaced ~1 cm apart (Fig. 1). Keratin in baleen never air-dries (Werth *et al.*, 2016a) but is stiffened by species-specific calcification patterns (Szewciw *et al.*, 2010). Plates erode on the medial (lingual side), producing hair-like baleen fringes (bristles). Fringes interlock to form a fibrous mat (Werth, 2013), but both plates and fringes are exposed to flow and together comprise the filter system (Werth & Potvin, 2016; Jensen *et al.*, 2017).

Just as Cuvier famously declared that he could deduce an animal's lifestyle from its tooth, it has likewise long been recognized that baleen of different whale species varies according to ecology. Tomilin (1954) and Nemoto (1959, 1970) recognized a fundamental dichotomy of mysticetes into major guilds: 'skimmers' separate copepods or other tiny plankton from a continuously filtered, swimming-induced stream, whereas 'gulpers' (which Nemoto called 'swallowers') intermittently engulf a single mouthful of water containing forage fish or larger plankton, especially krill (Pivorunas, 1979; Lambertsen, 1983; Cade *et al.*, 2016). Tomilin and Nemoto's 'skimmer'/'gulper' labels are simple and evocative yet misleading: skimming implies surface filtration, yet balaenids often feed deep in the water column (Simon *et al.*, 2009). For clarity and brevity, we instead use contrasting terms 'balaenid' (referring to right and bowhead whales, family Balaenidae) and 'rorqual' (including groove-throated rorquals, Balaenopteridae, plus the grey whale, *Eschrichtius robustus*). Whether 'rorqual' engulfment involves ram lunges (true rorquals) or suction (grey whale), intake is intermittent: the mouth encloses an engulfed water mass, which is then filtered. Continuously ram filtering balaenids have exceptionally long, finely fringed baleen, whereas shorter 'rorqual' baleen has coarser fringes (Werth, 2001, 2004; Werth *et al.*, 2016b; Young *et al.*, 2015). Balaenid filtration is a slow, steady-state process, whereas rorquals' dynamic ram lunges involve acceleration to high speed and rapid deceleration due to drag incurred by oral pouch expansion during engulfment (Potvin *et al.*, 2009).

Given the primacy of intraoral filtration to Mysticeti and this obvious difference in prey size, it is surprising that filter capacity has received scant attention. Nemoto (1970: 248) concluded that 'The relation between food concentrations and filtering volumes of baleen whales may be the key in solving the question of feeding of these large animals.' He gave 'approximate filtering areas' of different species, ranging from 1.7–4.6 m^2 in

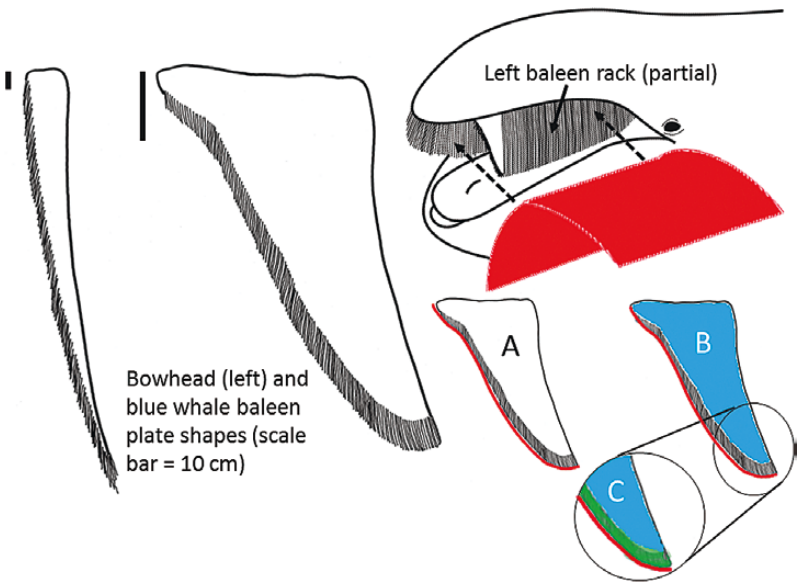

Figure 1. Schematic diagram showing triangular shape of individual baleen plates and their arrangement in paired comb-like racks suspended from the palate. Filter area was calculated via three approaches: A, 2D model = inner (medial) surface of each rack, with a tent-like form covering baleen's interior surface, shown in red; B, 3D model = 2D model plus flat plate surfaces (blue); C, 3D+ model = 3D model plus combined area of all free fringes (green).

rorquals to 13.5 m^2 in the right whale. Unfortunately, Nemoto (1970) provided no explanation for how these numbers were derived, nor did he indicate the sources from where they were obtained (apart from one estimate by Kulmov, 1966). Kawamura's wide-ranging monograph on the sei whale, *Balaenoptera borealis*, offered a means to quantify filter area (Kawamura, 1974); this was expanded by Sekiguchi *et al.* (1992), including data from Lambertsen *et al.* (1989). Unfortunately, Kawamura's 1974 calculation and subsequent (Kawamura, 1980) analysis involve just the two-dimensional inner margin of the baleen racks: 'the mesh formed by the woven bristles'. Although this is a logical place with which to begin filter quantification, more realistic measures include all areas contacting a filtered medium (in this case 'wetted') or otherwise separating particulate matter from flow.

Baleen area is often defined as the projected area of the mat created by exposed baleen fringes (Jensen *et al.*, 2017). Therefore, scaling of this surface in the context of first principles suggests that larger whales may suffer decreased performance in terms of filter time in rorqual lunges (Goldbogen *et al.*, 2012a) or via the mechanical power required to drive continuous ram filtration (Alexander, 1998). However, Alexander (1998) notes that if baleen scales differently or exhibits fractal geometry, some of these detrimental scaling effects could be ameliorated.

This study (1) presents a three-tiered approach of progressively cumulative detail for calculating realistic filter area (A_F), along with filter output flow rates and corresponding pressure differentials; (2) integrates these results with tag data from feeding whales in a thorough ecological analysis; (3) relates A_F to physical indices via morphological analysis; and (4) combines all information to consider phylogenetic and ecological evolution of mysticete filtration.

MATERIAL AND METHODS

Filtration area calculations

Starting with limited data within published literature for baleen filter surface area (A_F), this study derived more accurate A_F calculations. These depend on measurements not from idealized models but actual whale specimens of known body length (L_B). Measurements were obtained via necropsy. Wherever possible we took measurements from whole carcasses with two full baleen racks, using methods of Williamson (1973), Pivorunas (1976) and Young (2012) to measure baleen plates, count fringes and calculate fringe density. In a few cases we used single-rack museum specimens and doubled our values, presuming both racks are of equal size (confirmed by examination and calculations of specimens with dual racks).

Williamson (1973) presented the first account of baleen A_F and contrasted 'standard filter area' [a rough two-dimensional (2D) estimate] with 'true filter area' (taking into account rack curvature), which he did not measure. He determined standard A_F by projecting photographs of racks onto graph paper; from this he computed a formula of A_F = rack length × longest plate length × a coefficient k (approximating curvature along the fringed medial surface, determined from photographic analysis and varying by L_B). He concluded that k equals 2.2–2.7 in *Balaenoptera* and ~1.5 in *Eubalaena* (lower coefficient due to straighter baleen), but this coefficient remains something of a mystery 'fudge factor'.

Our study initially followed Kawamura's (1974) technique because it offers a simple procedure to calculate A_F. This involves estimating the filter as a 2D surface like a window screen creased along the palate. More accurately, the baleen filter can be compared to a tent-like structure's interior face, with walls comprising the frayed medial surface of all plates in two facing racks (Fig. 1). Whereas the outer (lateral or labial) margins of baleen plates are nearly straight, the inner margins needed to calculate surface area are curved. Kawamura's origami-style solution was to approximate this curved inner surface with a series of line segments whose length varies by position on a plate and along a rack. Kawamura (1974) thus 'unfolded' a rack, documenting its curved interior margin as a series of splines. With spline lengths totalled for two full racks, total filter area is obtained. Kawamura (1974) measured plate/fringe dimensions but they did not enter his A_F estimation, which remained strictly 2D (albeit arched).

Although Kawamura's 2D approach (Kawamura, 1974, 1980) has utility, a more complex method is needed to accurately portray baleen's true 3D topography and, crucially, to include the filter's total wetted surface area, including plate faces and fringes. Therefore, our second approach expanded this 2D model by adding combined planar dimensions of individual plates. For baleen, this involves calculating the planar area of each anterior/posterior face for each plate (Fig. 1). Plate dimensions vary, so measurements were incrementally taken for every fifth plate within a rack from the most anterior to most posterior plate. The basic 3D model combined plate areas (calculated from photos using ImageJ) with updated data from the 2D model (also using ImageJ to determine splines). Finally, an enhanced (3D+) model incorporated a third element: total surface area of all fringes on all plates throughout both racks of a whale's mouth (Fig. 1). Fringes were treated as basic cylinders of uniform diameter (a valid assumption confirmed by digital caliper measurements along the length of 60 fringes). Because tapering is minimal, each cylinder's surface

area was computed based on fringe length. Hence starting with the rack's interior mat surface (=the 2D model), successively detailed and progressively nested models incorporated combined areas of plate faces (=3D model) and fringe areas (=3D+; Fig. 1). Although hydrated baleen is flexible (Werth *et al.*, 2016a) and its porosity varies with flow speed and volume, drag and other dynamic parameters (Werth, 2013; Werth & Ito, 2017), total A_F was measured as a fixed, static value for this study using morphometric calculations outlined above.

Ten species were surveyed: *Balaenoptera acutorostrata* (common minke whale; ten specimens used for 2D analysis, six for 3D/3D+ analyses), *B. borealis* (sei whale, 17/6 specimens), *B. edeni* (Bryde's whale, 32/4), *B. musculus* (blue whale, 5/5), *B. physalus* (fin whale, 30/15), *Megaptera novaeangliae* (humpback whale, 5/4), *Balaena mysticetus* (bowhead whale, 9/6), *Eubalaena glacialis* (North Atlantic right whale, 5/5), *Eschrichtius robustus* (grey whale, 3/3) and *Caperea marginata* (pygmy right whale, 4/3). Data for all three models (2D, 3D, 3D+) were plotted against body length (L_B), adding published A_F data (2D only) to our previously unpublished data. Baleen A_F was compared with morphometric parameters such as the size of the lips, palate and jaws (from field necropsy or museum specimens) as well as tag data (e.g. swim speed during filtration) for whales of varying body length (L_B).

Filter output flow rate and pressure estimates

We constructed a mathematical model of filter output flow rates to compare continuous and intermittent filtration using morphometric information (plate thickness, width of intra-baleen or IB gap, number of plates/rack) and tag-recorded data from feeding whales (speed and duration of engulfment and purging/expulsion, etc.). A first equation describes the flow speed (U_{out}^{rorq}) output of a rorqual's baleen rack during the expulsion/purge stage following a lunge. It is calculated from conservation of the volumetric flow rate through a whole baleen rack in which the through-baleen flux, namely U_{out}^{rorq} times the total area of the gaps comprising a rack, is equal to half the engulfed water volume (V_{engulf}) divided by purge time (t_{purge}). Purge time was determined from tagged whales from the end of engulfment until the start of positioning for a subsequent lunge (Cade *et al.*, 2016); engulfed volume is expressed as the product $f M_c/\rho$, in terms of the known body mass (M_c), seawater density (ρ) and engulfed volume fraction (f) (Goldbogen *et al.*, 2012a). With the total IB gap area along each rack obtained from the product of the number N_{plate} of baleen plates (per rack) and the averaged gap area A_{gap} between two neighbouring plates, the full equation is:

$$U_{out}^{rorq} = \frac{\frac{1}{2} \cdot f \cdot (M_c / \rho)}{N_{plate} A_{gap}} \cdot \frac{1}{t_{purge}} \quad (1)$$

The flow speed output of a balaenid rack (U_{out}^{bal}) is calculated similarly, but in this case through comparison of the flux entering half of the oral apparatus of area assumed equal to $\frac{1}{2} D_{in} h_{HT}$, with D_{in} as the mouth inlet width and h_{HT} the mean baleen height (assuming foraging at depth; Potvin & Werth, 2017) vs. the flux exiting one of the racks, through total gap area $N_{plate} w_{gap} h_{HT}$. With the entering flux based on a whale's forward speed U_{whale} (assuming minimal bow wave deceleration of entering flow), the speed U_{out}^{bal} characterizing exiting flux is given by:

$$U_{out}^{bal} = U_{whale} \frac{\frac{1}{2} D_{in}}{w_{gap} N_{plate}} \quad (2)$$

Values for U_{whale} are estimated to range from 0.6 to 1.5 m s^{-1} (Simon *et al.*, 2009; Werth & Potvin, 2016; Goldbogen *et al.*, 2017). Note that here the mouth's inlet width D_{in} varies according to gape and lip canting angle (Potvin & Werth, 2017) and is assumed as D_{in} = 0.70 m to simplify all calculations. This is currently an uncertain input for which no field data exist.

Finally, to examine effects of viscous shear forces applied by water flowing against wetted surfaces of baleen, an estimate of the pressure gradient (ΔP) needed to push water through IB gaps is calculated as follows, using concepts and data from pipe hydraulics (Fox & McDonald, 1978; Blevins, 1984):

$$\Delta P = K \frac{1}{2} \rho U_{out}^2 \quad (3)$$

The so-called friction coefficient K encapsulates energy-dissipating effects of both viscous friction and flow turbulence within pipe flow, as applied here to channels created by IB gaps. This flow may be pictured as entering each gap from a direction roughly parallel to the gap's axis, then making a sharp 90° bend dorsally (rorquals) or posteriorly (balaenids) on exit, upon being deflected by the lip (Potvin & Werth, 2017; Goldbogen *et al.*, 2017). This bend generates secondary flows (vortices, mainly) which significantly increases the value of K at low values of the pipe's diameter-based Reynolds number (Re_D). This diameter equals the gap's hydraulic diameter, defined as $2 w_{gap} L_{span} / (w_{gap} + L_{span})$. Blevins (1984: 55–57) estimates K as $\sim K_{bend} + f L_{chord} / D$, with the friction factor f accounting for viscous friction along the straight portion of a pipe, thus estimated as 0.10 (balaenids) and 0.04 (rorquals) (Fox & McDonald, 1978; Blevins, 1984). The difference

in f is the direct consequence of higher IB Reynolds numbers in rorquals (Re_D > 4000) in comparison to balaenids (Re_D ~ 1000), following significantly differing values of U_{out} (as explained in the Results). The ratio L_{chord}/w_{gap} accounts for the increasing friction arising with narrower IB gaps, along with f and its dependence on Re_D. The other friction term K_{bend} accounts for the bend's secondary flow losses (Blevins, 1984), which at the relevant Re_D yields K_{bend} = 0.024–0.052 (rorquals) and 1.00 (balaenids). In those estimates L_{chord} is the average width (chord) of a typical baleen plate. Values for w_{gap} are obtained from the literature (Young, 2012) and from morphometric data taken from actual baleen plates (for A_F calculation outlined above); values for L_{chord} are adjusted to a rack's wetted area, similar to the difference between our 2D and 3D A_F calculations (i.e. with L_{chord} being two times the mean baleen length h_{HT}).

RESULTS

A clear correlation exists between A_F and L_B, with sharply differing A_F of balaenids and 'rorquals' as revealed by all three models. Figure 2 displays results of the basic 2D analysis, with A_F ranging from 0.38 m² in a 3.3-m pygmy right whale to 7.42 m² in an 18-m bowhead (a 20-fold difference; 3.6× corrected for L_B). Within each species, A_F increases almost linearly with L_B. There is marked separation between continuously filtering balaenids and intermittently filtering rorquals/grey whales, although minke whales are on a 'bend' at the lowest end of the otherwise linear 'rorqual' relationship. Sei whales occupy a precisely intermediate A_F position, and pygmy right whales are aligned with true right and bowhead whales by 2D analysis (Fig. 2). Table 1 shows regression results for all models, with linear, polynomial (quadratic) and allometric (power curve) equations (Packard, 2013, 2017) for filter area y (m²) per unit body length x (m).

When plate surfaces are incorporated into filter calculation (3D model; Fig. 3) the overall relationship between A_F and L_B remains, as does falling of taxa into balaenid/'rorqual' groups. However, balaenids are best approximated by a power curve; 'rorquals' also fit better along a polynomial curve, although less so on the small L_B end (relative to 2D analysis). Unlike the outcome of 2D analysis, the 3D model aligns pygmy right whales with 'rorquals' rather than with balaenids (Fig. 3). This is also the case with the enhanced 3D+ model (Fig. 4), which yields results nearly identical to the 3D model apart from somewhat larger A_F calculation incorporating free fringe areas. For all three models, log–log plots (Figs 2–4) reveal similar scaling of A_F and L_B, with near-identical slopes (exponents) for the three discrete groups. Not only is there distinct divergence between balaenid/'rorqual' and sei whale groups, but there is essentially no intraspecific variation apart from L_B (i.e. individuals within each species fit along a line), with clear overlap between species (e.g. smallest blue and largest fin whales).

Although the overall relationship between A_F and L_B is similar for all three models, a notable difference is that data of 3D and 3D+ models (Figs 3, 4) yield, for balaenids and 'rorquals', distinct regression lines (Table 1) that do not intersect. In contrast, in the simplest (2D) model (Fig. 2), filter areas of these two groups converge at a body length of 4.68 m. However, in all analyses (2D, 3D, 3D+; Figs 2–4) the sei whale's intermediate position converges with the 'rorqual' consensus line at L_B = 5.37 m.

Filter output flow speed values (U_{out}^{rorq}) have been estimated at 0.6–0.7 m s^{-1} among the largest rorquals

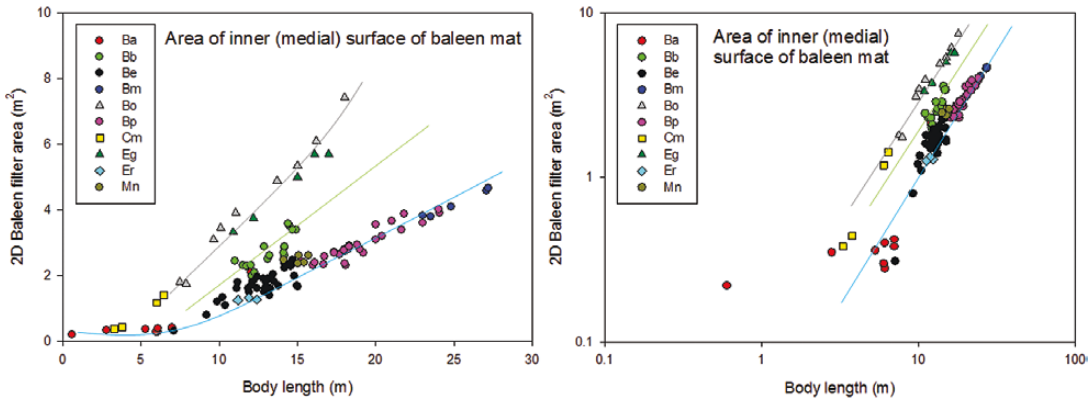

Figure 2. Filter area (from 2D model using only inner mat surface) plotted against body length, with quadratic curve fit showing balaenids (solid line) vs. 'rorquals' (true rorquals plus grey whale; dashed line) and intermediate position of sei whale (dotted line). The same data are presented in a log–log plot at right. Rorquals are represented by circles, balaenids by triangles, neobalaenid by squares and grey whale by diamonds. Ba = minke whale, Bb = sei, Be = Bryde's, Bm = blue, Bo = bowhead, Bp = fin, Cm = pygmy right whale, Eg = right, Er = grey, Mn = humpback.

Table 1. Regression equations (linear and curve fit) relating baleen filter area (y) to body length (x)

Model	'Skimmer'	Sei	'Gulper'
2D (linear fit)	$y = 0.466x - 1.63$ ($R^2 = 0.95$)	$y = 0.321x - 1.52$ ($R^2 = 0.66$)	$y = 0.191x - 0.66$ ($R^2 = 0.94$)
2D (quadratic)	$y = 0.418x + 0.002x^2 - 1.63$ ($R^2 = 0.96$)	—	$y = 0.159x + 0.001x^2 - 0.66$ ($R^2 = 0.95$)
2D (allometric)	$y = 1.03x^{0.11}$ ($R^2 = 0.94$)	—	$y = 0.66x^{0.08}$ ($R^2 = 0.89$)
2D (log, power)	$y = 0.10x^{1.47}$ ($R^2 = 0.99$)	$y = 0.04x^{1.63}$ ($R^2 = 0.82$)	$y = 0.06x^{1.31}$ ($R^2 = 0.93$)
3D (linear)	$y = 12.95x - 20.63$ ($R^2 = 0.92$)	$y = 9.761x - 23.02$ ($R^2 = 0.98$)	$y = 4.145x - 11.964$ ($R^2 = 0.89$)
3D (quadratic)	$y = -27.26x + 1.43x^2 + 252.96$ (R^2 0.97)	—	$y = -1.548x + 0.19x^2 + 23.24$ ($R^2 = 0.97$)
3D (allometric)	$y = 48.94x^{0.08}$ ($R^2 = 0.95$)	—	$y = 12.11x^{0.09}$ ($R^2 = 0.96$)
3D (log, power)	$y = 0.64x^{1.23}$ ($R^2 = 0.91$)	$y = 4.67x^{1.21}$ ($R^2 = 0.93$)	$y = 1.03x^{1.40}$ ($R^2 = 0.97$)
3D+ (linear)	$y = 13.791x - 22.16$ ($R^2 = 0.92$)	$y = 9.710x - 21.760$ ($R^2 = 0.97$)	$y = 4.145x - 11.592$ ($R^2 = 0.90$)
3D+ (quadratic)	$y = -29.09x + 1.53x^2 + 269.65$ ($R^2 = 0.97$)	—	$y = -1.448x + 0.189x^2 + 23.20$ ($R^2 = 0.97$)
3D+(allometric)	$y = 52.0x^{0.08}$ ($R^2 = 0.95$)	—	$y = 12.50x^{0.09}$ ($R^2 = 0.96$)
3D+ (log, power)	$y = 6.64x^{1.23}$ ($R^2 = 0.91$)	$y = 4.67x^{1.21}$ ($R^2 = 0.97$)	$y = 1.03x^{1.4}$ ($R^2 = 0.93$)

(Fig. 5, Table 2), but the large range in purge time (Fig. 5) may widen this scale considerably both between and within individuals (i.e. on a lunge-to-lunge basis). Nonetheless, these values are about ten times those of balaenid filtration output flows speeds (U_{out}^{bal}). This disparity is due to significantly differing filter area (Figs 2, 3). Interestingly, both groups of outflow speeds vary little with body size (L_B), as made clear by the allometry of eqns 1 and 2. For rorquals, engulfed volume scales roughly with L_B^3 while each baleen gap area (A_{gap}, through which purged water flows) roughly varies as L_B^2. Combining both values in eqn 1 yields a near-linear growth in L_B which is cancelled out by a similar linear scaling in purging time t_{purge} (Fig. 5). With balaenids a similar scaling insensitivity also arises, from the ratio in eqn 2 of the mouth inlet width (D_{in}) to IB gap width (w_{gap}). From baleen dimensions (Table 2), eqn 3 yields friction coefficient K values of 0.89 (blue whale), 0.44 (humpback whale) and 1.55 (balaenids); the last is consistent with K for a balaenid rack in higher resolution modelling (Potvin & Werth, 2017). At outflow velocities estimated above, rorqual IB gap pressure ranges from 90 Pa (humpback whale) to 190 Pa (blue whale) vs. 2.59–2.87 Pa for balaenids.

DISCUSSION

DIVERGENT CONTINUOUS/INTERMITTENT FILTRATION STRATEGIES

There is clear divergence between balaenids and 'rorquals' (Balaenopteroidea = grey + rorqual whales) and little variation within groups (Figs 2–4). Our analysis of filtration strategy thus supports the long-standing contention of disparate mysticete ecological guilds (Tomilin, 1954; Nemoto, 1959, 1970), with balaenids employing a filter surface four to five times larger than that of similarly sized balaenopteroids. Although previous reports highlighted taxonomic differences in relative filter 'coarseness' or porosity (Mayo *et al.*, 2001; Werth, 2004, 2013) and related it to dietary differences (tiny plankton for balaenids, larger plankton and fish for 'rorquals'), there has been only limited investigation of mysticete filter area (Kawamura, 1974, 1980; Sekiguchi *et al.*, 1992) and few studies have quantitatively related baleen area to filter-feeding modality.

Equations relating A_F to L_B (Table 1) can be calculated for individual mysticete species but there is little utility in doing so, as they are virtually identical to overall (group) formulae. Furthermore, there is strikingly little variation within species. Unlike cetacean species with distinct ecotypes and morphotypes (e.g. the killer whale, *Orcinus orca*; Riesch *et al.*, 2012; McCurry *et al.*, 2017), mysticetes display no such variation

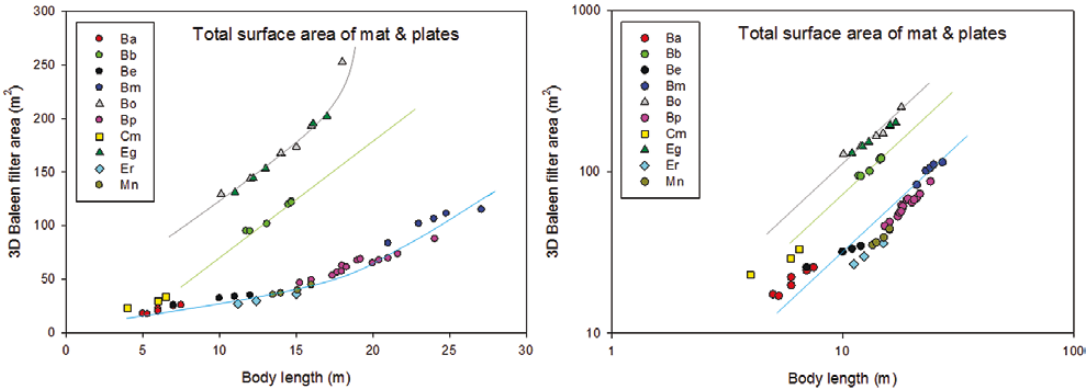

Figure 3. Linear and log–log plots of filter area (from 3D model incorporating plate face area) plotted against body length, with allometric curve showing continuous ram-filtering balaenids (grey line) vs. quadratic curves of intermittent-filtering rorquals and grey whale (blue line) and sei whale (green line). Abbreviations/symbols as in Figure 2.

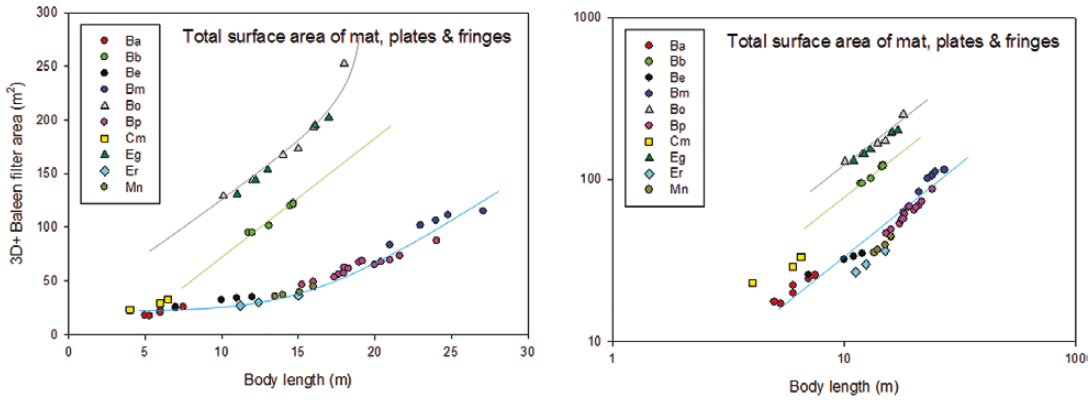

Figure 4. Linear and log–log plots of filter area (from 3D+ model with plate face and free fringe surface area) plotted against body length, with allometric curve showing continuous ram-filtering balaenids (grey line) vs. quadratic curves of intermittent-filtering rorquals and grey whale (blue line) and sei whale (green line). Abbreviations/symbols as in Figure 2.

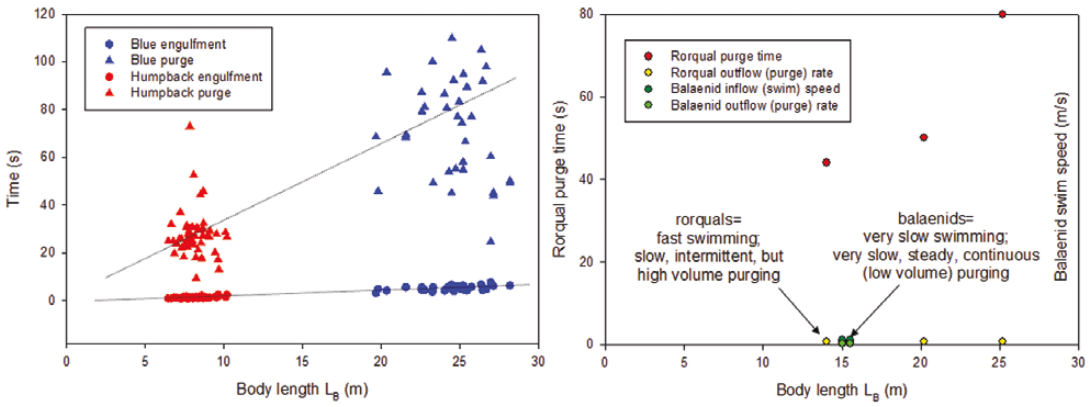

Figure 5. Tag data from feeding whales reveal differing filter strategies based not only on differing prey but also on hydrodynamics of filtration, involving capture and purging/expulsion of filtered water (i.e. speed and force of water entering and exiting the mouth). Left panel shows rorqual purging, like engulfment, scales with L_B but with much higher slope due to proportionally larger filter. Right panel shows slight difference between balaenid capture/purge flow speeds but large discrepancy for rorquals (see also Table 2), indicating that purge (=filtration) time limits filter area.

Table 2. Mathematical modelling results of outflow speed and friction (NA, not applicable; –, data unavailable)

Species and N_{plate}	L_B (m)	L_{thick} L_{span} L_{chord} (m)	A_F (2D) (m^2)	w_{gap} (m)	Hydraulic diameter D (m)	f & M_c (1000 kg)	t_{purge} (s)	U_{whale} (m s^{-1})	U_{out} (m s^{-1})	IB gap Re_D	L_{chord}/D	K	ΔP (Pa)
Right 320	15.0	0.0033 2.10 0.10	2.60	0.015	0.03	NA 56.0	NA	0.8	0.058	1183	3.35	1.50	2.59
Right 320	15.0	0.0033 2.10 0.10	2.60	0.01	0.02	NA 56.0	NA	1.2	0.132	791	5.02	1.50	2.59
Bowhead 315	15.5	0.0037 2.30 0.11	2.75	0.015	0.03	NA 56.0	NA	0.8	0.060	1224	3.69	1.55	2.87
Bowhead 315	15.5	0.0037 2.30 0.11	2.75	0.01	0.02	NA 56.0	NA	1.2	0.134	818	5.52	1.55	2.87
Blue 315	25.2	0.0031 0.80 0.21	4.1	0.0050	0.010	1.4; 96.6	80	NA	0.64	4418	20.9	0.89	190.3
Fin 360	20.2	0.0025 0.70 0.15	2.9	0.0033	0.006	1.3; 47.0	50	NA	0.72	3219	23.1	—	—
Sei 300	17.0	0.0026 0.70 0.14	4.5	0.0074	0.014	NA; 28.0	NA	NA	—	—	9.6	—	—
Bryde's 290	13.5	0.0025 0.50 0.12	2.0	0.0044	0.008	NA; 22.0	NA	NA	—	—	13.8	—	—
Minke 270	8.0	0.0018 0.40 0.12	0.4	0.00005	0.00014	NA; 9.65	NA	NA	—	—	1157.3	—	—
Humpback 305	14.0	0.0017 0.60 0.10	2.4	0.0048	0.010	1.1; 46.2	44	NA	0.63	4177	10.4	0.44	90.4

apart from allometric increases in A_F with L_B. A small but notable exception involves rotund yearling (*ingutuk*) vs. slimmer subadult (*qairilik*) bowheads, where disproportionate investment in filter growth early in life history allows greater nutrient intake in preparation for rapid skeletal growth (George *et al.*, 2016), which aids in thermoregulation of this polar species. When only bowheads are plotted, smaller (younger) whales have slightly disproportionally larger A_F. Similar ontogenetic trajectories may exist in rorquals (Tsai & Fordyce, 2014a, b).

Numerous morphological features that further distinguish continuous/intermittent filterers (Table 3, Fig. 6) clearly relate to this ecological divergence. Although baleen fundamentally operates identically in all mysticetes, by separating retained bulk prey from expelled seawater, in fact prey are collected entirely differently. Balaenids collect prey via slow, steady-state, ram-induced filtration, most likely involving cross-flow filtration (Werth & Potvin, 2016; Potvin & Werth, 2017), whereas 'rorquals' intermittently engulf a volume of water that is then expelled. In grey whales, baleen both captures and retains prey; in rorquals baleen retains prey caught by the expanded buccal cavity and swallowed after water is filtered through baleen (Goldbogen *et al.*, 2017). Coarser 'rorqual' fringes may relate not only to larger prey, as commonly assumed, but also to stronger filtration outflows (Table 2), with thicker fringes better resisting damage. Wearing of plate margins has historically been presumed to arise from rubbing by the tongue (Werth, 2001), but a cross-flow mechanism without scraping is less likely to clog (Brainerd, 2001), and mechanical demands of filtration/expulsion alone are sufficient to abrade plates (Werth *et al.*, 2016b). Higher rorqual purging (expulsion) speeds may create additional fringes,

Table 3. Comparison of body and filter features (average; centre of baleen rack) in adult whales

Trait	Balaenid	Sei	'Rorqual'
Number of plates per rack (range)	300 (240–390)	320 (220–400)	275 (230–400)
Plate length (cm)	296	77	72
Plate thickness (cm)	0.34	0.26	0.24
Plate density (per cm)	1.02	1.35	1.18
Fringe length (cm)	9.39	7.22	4.68
Fringe diameter (cm)	0.16	0.12	0.44
Fringe density (per cm)	52	46	21
Fringe type	Long, fine, flexible	Long, fine, flexible	Short, stiff, coarse
Baleen plate form	Long, thin, narrow; hang straight down; Slightly curved plates	Intermediate plate form and position; less curve than 'rorqual'	Short, wide plates angled outward; curved cross-section
Overall body form	Rotund	More robust than other rorquals, with thicker tail stock*	Slender
Flippers & flukes	Broad; squarish	Intermediate aspect ratio*	Long and slender
Dorsal fin	None	Large	Small
Rostrum	Sharply arched	Slightly arched	Flat and broad
Mandibles	Strongly curved	Slightly curved	Less curved
Palate	Flatter keeled vomer	Mid-size keel	Pronounced keel
Lip	High, muscular	Mid-size, muscular	Very low; little muscle
Tongue	Muscular, firm	Firmer than 'rorqual'	Floppy, flaccid
Ventral grooves	None	Fewer, shorter	Many, long

*From Brodie & Vikingsson (2009).

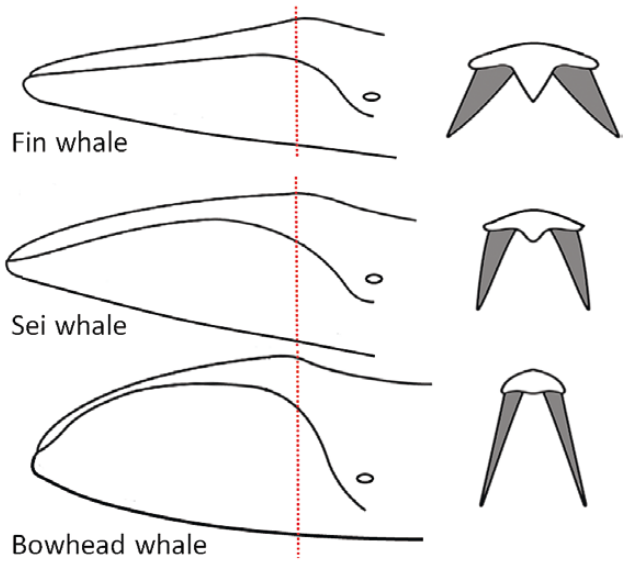

Figure 6. Comparison of fin, sei and bowhead whales in profile and cross section (at rostral peak, dashed lines), redrawn from concept by Brodie & Vikingsson (2009). Sei whale has intermediate head shape and other feeding morphology including rostral arch and raised lip, thinner rostrum, less prominent palate, and longer and more vertically orientated baleen plates.

thereby increasing both A_F and drag, further limiting the ceiling for rorqual purge rates.

Flow biomechanics and energetics

The basic rorqual/balaenid dichotomy relates not solely to prey type and size but especially to biomechanics of filtration and drag forces. Given that drag increases as the square of velocity, ram-driven filtration (from locomotor propulsion) of a fine, low-porosity filter with high A_F requires low swimming speeds to avoid extreme drag and unsustainable metabolic expenditure (Potvin & Werth, 2017). Higher swimming/foraging speeds might also force accumulated prey through the filter. Tag data indicate balaenid foraging speeds of < 1 m s^{-1} (Simon *et al.*, 2009), much slower than 2–5 m s^{-1} swim speeds recorded during rorqual engulfment (Goldbogen *et al.*, 2006, 2013, 2017; Simon *et al.*, 2012; Cade *et al.*, 2016). On the other hand, lunges incur greater mass-specific energy and power expenditure but are economical, relative to continuous ram filtration, in yielding higher volumes of larger, more elusive prey (Goldbogen *et al.*, 2017). With their substantially lower A_F, rorquals can swim with open gape much faster than balaenids, which are limited to low foraging speeds. Balaenids capture smaller, less agile and less energy-dense prey (Werth, 2012), whereas rorquals chase – and

quickly ingest – high quantities of energy-dense prey (Leaper & Lavigne, 2007; Michaud & Taggart, 2007). With their more rapid (40–60 s) filtration (Fig. 5) and overall higher swimming speed (Table 2), rorquals can consume highly patchy prey separated by long distances. Discrete rorqual filtration events have high engulfment capacity, but filtration of the engulfed volume is potentially at a lower performance in absolute water filtered per unit time (Simon *et al.*, 2012; Goldbogen *et al.*, 2013). We calculate roughly 1750 kg water filtered s^{-1} for a 100 000-kg blue whale vs. 2250 kg s^{-1} for a 15-m right whale. Lower volumetric flow performance is presumed to be allowable because prey are caught in the mouth (assuming high capture efficiency of the filter itself), precluding prey escape, and because rorquals probably feed on higher quality prey patches (Hazen *et al.*, 2009; Goldbogen *et al.*, 2011, 2015), so that energetic gains may be higher despite lower filtration rates.

Previous studies investigated scaling of rorqual engulfment capacity (Goldbogen *et al.*, 2010, 2011, 2012a, b; Potvin *et al.*, 2012; Friedlaender *et al.*, 2014). In general, mass-specific engulfment capacity increases with L_B in rorquals due to positive allometry of the engulfment apparatus (Goldbogen *et al.*, 2010, 2012a). Equation 1 suggests the output flow rate, driven by the ratio of engulfed volume to baleen area, is tempered by shorter filtration/purging times (relative to balaenids) in order to meet energetic demands of engulfment and O_2 availability during dives; it may also be limited by power supplied by muscles associated with ventral groove blubber during purging (i.e. the pressure that muscles create to move water through the filter). Engulfment costs, increasing as $L_B^{3.6}$ (Potvin *et al.*, 2012) in comparison to O_2 storage (L_B^3; Goldbogen *et al.*, 2012a), must constrain purging time to negatively allometric scaling (~L_B; Fig. 5) and thus to size-insensitive filter flow rate output.

Our methods also highlight the (lateral) pressure difference across baleen (ΔP) which a whale must work against to drive the filtration process. In rorquals, high ΔP requires high forces from muscles lining the expandable oral pouch and driving its emptying (Shadwick *et al.*, 2013). In contrast, a much lower balaenid ΔP can be generated by lower ram speeds (Table 2).

Is this central disparity merely reflective of alternative foraging choices (low-speed filtering of less mobile prey vs. high-speed lunges of more mobile prey) or is it necessarily imposed by physical and metabolic demands of divergent evolutionary strategies? The disparity may be due to both factors. Even though balaenids swim more slowly than rorquals while foraging, their energetic demands come from the high drag generated while propelling a huge filter (Potvin & Werth, 2017). In contrast, rorquals' main energy expenditures come from high-speed swimming during engulfment rather than during filtration (purging), a stage executed at lower speeds. In rorquals the overwhelming energetic requirements of engulfment (Potvin *et al.*, 2012) and limits on O_2 storage (Goldbogen *et al.*, 2012a) must drive the timing of foraging. Such requirements probably limit baleen to short plate lengths (span) compared to that of balaenids, to reduce overall body drag during mouth opening. However, this also entails higher baleen throughput flows and cross-baleen pressure differences, generating higher costs during filtration. Such costs, however, are still lower than those incurred during the remainder of a lunge, as filtration is not ram-powered via fluking, but internally powered via muscle contraction (although the elastic recoil of ventral groove blubber makes this faster and easier). Thus, although A_F scales with body size for both strategies (Figs 2–5), it may scale in differing ways due to costs of filtration being dominant in balaenids but secondary in rorquals. The large difference in friction coefficient K among rorquals arises from baleen morphology (longer baleen span to IB gap in blue whales); the 20–40-fold difference between K for rorquals and balaenids stems from much greater outflow speeds in rorquals affecting both ΔP (eqn 3), the gap's Reynolds number (Re_D) and K. Interestingly, heightened pressure differences emphasize the necessity for rorquals to keep overall baleen surface area small in comparison to balaenids.

Balaenids and rorquals have strikingly different forms, not just of the filtering apparatus but of the entire body (Table 3). A 15-m bowhead has a mass of 56 100 kg, 2.7 times that of a 15-m fin whale (20 850 kg, based on data from Schultz, 1938; Nishiwaki, 1950; Lockyer, 1976; George *et al.*, 2007; Fortune *et al.*, 2012). We used body length rather than body mass (M_B) as a measure of size because lengths are more readily available: it is easy, and hence standard practice, to measure L_B during post-mortem analysis, whereas it is difficult to weigh a whale, particularly a large adult. However, M_B could offer a better comparison for filter area given that A_F supports the body's metabolism, making energetic analysis more apt. Plots of A_F vs. body mass (Fig. 7) further demonstrate balaenid/'rorqual' filtration strategies supporting divergent morphology/ecology, and further reveal the sei whale as a balaenopterid with balaenid-like filtration.

Sei whale filtration

In phylogenetic terms, it is interesting that balaenids are basal forms – the probable outgroup for all other extant Mysticeti (Nikaido *et al.*, 2006). Whether the slow, high-area continuous filtration strategy preceded the 'rorqual' strategy remains an open question. Regardless, sei whales appear to present a partial transition

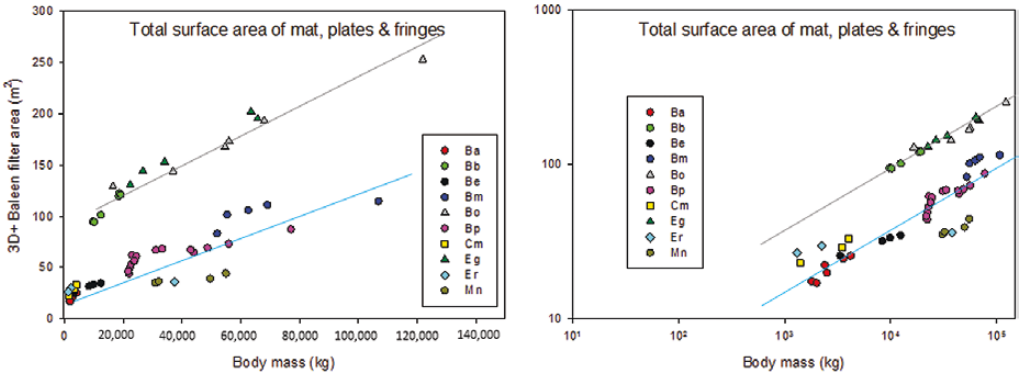

Figure 7. Linear and log–log plots of 3D+ filter area (compare with Fig. 4) plotted against body mass instead of length.

to continuous filtration, with some ecological and morphological characters of the sei whale head, body and filter converging on those of balaenids (Fig. 6, Table 3). Sei whale baleen is longer and more finely fringed than in other rorquals (Horwood, 2017). It is clear sei A_F does not fit that of other balaenopterids (Figs 2–4, 7).

Given the sei whale's dietary difference from other rorquals (preferring copepods or other small zooplankton) and its apparent propensity for balaenid-type feeding (Kawamura, 1980), it is not unexpected that its filter size would not fall on the same curve with other 'rorquals' (Figs 2–4). The slope (exponent) of its A_F vs. L_B relationship mirrors that of balaenids, but falls in a position precisely intermediate between the two established guilds, although it is unclear whether this reflects an intermediate functional design. When plotted against body mass (Fig. 7), the sei whale filter aligns perfectly with balaenids. Not only has its filter strongly diverged from that of other balaenopterids in porosity (fineness), length and position within the mouth (Fig. 6), but the sei whale's body demonstrates modification of the sleek, trim rorqual form, with a somewhat thicker, more robust body that may now be adapted to better serve high-drag filtration (Table 3), including a thicker tail stock plus modified control surfaces (shorter and stubbier flippers and flukes; a larger dorsal fin) to prevent roll and aid in propulsion (Brodie & Vikingsson, 2009). Other analyses of body form (Ahlborn *et al.*, 2009) indicate congruity of sei whales with other balaenopterids. However, the sei whale could be at a competitive disadvantage within specific niches occupied by other rorquals and balaenids. Whereas the two guilds have bodies and filters reflecting partitioning of prey resources, the sei whale is a true generalist: it may use both rorqual and balaenid strategies (Horwood, 2017), but as a generalist it may suffer lower performance when employing either feeding mode. As Brodie & Vikingsson (2009) suggested, the sei whale's morphological intermediacy and ecological versatility enables it to exploit a wide range of prey in patches of varying size and density. Thus, *B. borealis* may be adaptable in different ecosystems or situations, but its intermediacy may also explain its limited distribution and smaller population size (even of pre-whaling stocks; Horwood, 2017) where it faces competition.

Regarding our hydrodynamic/biomechanical analysis, it is clear that whatever filtration strategy it follows, the sei whale's baleen alone suggests atypical kinematics and body energetics for either foraging mode. The IB gap between adjacent plates varies (Werth & Potvin, 2016), usually > 1 cm in balaenids vs. ≤ 1 cm in rorquals. Again the sei whale appears to be a functional intermediate, with plates more widely spaced than in other balaenopterids yet less than in balaenids. Filter outflow speeds for a 'skimming' sei whale could be higher than those of right/bowhead whales, but more data are needed to determine how sei whale lunge efficiency would compare to other rorquals. Unfortunately, although sei whale migratory patterns have been studied via satellite tagging (Olsen *et al.*, 2009), functional tag data are mostly lacking, with acoustic time–depth transmitters revealing diving patterns perhaps linked to diel vertical migration of copepods (Ishii *et al.*, 2017). Further data are needed to elucidate *B. borealis*'s filtration mode and role in mysticete ecological divergence.

Pygmy right whale filtration

Another species that stands out in our analysis is the pygmy right whale, *Caperea marginata*, which despite its name is not a miniature version of right whales (*Eubalaena* sp.). *Caperea* is classified in the monotypic family Neobalaenidae, although its slightly curved rostrum and lip are reminiscent of its namesake right whale. Fordyce & Marx (2013) argued that *Caperea*, the smallest mysticete, is a relict of the otherwise extinct cetothere lineage. Genetic evidence reveals a closer relationship to rorquals than to right whales (Nikaido

et al., 2006). Although tag data and functional studies are lacking, as in sei whales, stomach contents and limited field observations (showing no rapid lunges or wide gape behaviour) suggest the pygmy right whale filters copepods and krill (Kemper, 2017), perhaps in a manner similar to that of balaenids or the sei whale.

Unfortunately, our A_F analysis sheds little light on the potential ecology of this enigmatic species. *Caperea* fits neatly with balaenids by the simpler 2D filter area (Fig. 2), but more realistic 3D measures (Figs 3, 4, 7) align *Caperea* with 'rorquals.' Perhaps the pygmy right whale, like the sei whale, is best seen as an ecological intermediate that does not clearly fit within the two feeding guilds of Mysticeti. Again, kinematic data (on swim speed during filtration, etc.) might resolve this mystery.

Origin and evolution of mysticete filtration

Our data on filtration surfaces has potential applicability to the study of the origins of baleen, and of the ecology of the first baleen whales. The earliest mysticetes (Fitzgerald, 2010; Lambert *et al.*, 2017; Fordyce & Marx, 2018), including *Mystacodon*, *Llanocetus*, *Mammalodon* and several aetiocetid genera, all bore dentition, and although some palaeontologists allege the presence of proto-baleen in these lineages, based on spacing between teeth and putative palatal vasculature, the evidence for proto-baleen (Deméré *et al.*, 2008) is equivocal at best. Fossilized baleen is rare (Gioncada *et al.*, 2016; Marx *et al.*, 2017) and its appearance is highly altered due to taphonomic change, making it impossible to determine filter area even in derived fossil taxa with a 'full' baleen filter. Histological and molecular evidence indicate that baleen's development, and perhaps evolution, relates to genes shared with teeth (Thewissen *et al.*, 2017). Even if an early filter were present in original toothed mysticetes, it would almost surely not have had the elaborate size found in crown Mysticeti. Truly edentulous (=chaeomysticete) basal baleen whales, eomysticetids and cetotheriids (of which *Caperea* is a purported remnant; Marx & Fordyce, 2016), arose later in the mid- and late Oligocene. At least one of these lineages is presumed ancestral to extant mysticetes. Whether toothed or edentulous, all early mysticetes were of approximately the same body size (L_B = 4–5 m), as estimated from limited skeletal (mostly cranial) fossils (with the notable exception of *Llanocetus*, with an estimated body length of up to 8 m; Fordyce & Marx, 2018), which corresponds to the body size at which scaling trajectories of baleen area converge among different mysticete lineages (Fig. 2).

The feeding mode of the earliest mysticetes remains a mystery and is the subject of intense debate (Geisler *et al.*, 2017). Ancestral mysticetes may have used raptorial or suction feeding (Marx *et al.*, 2016; Hocking *et al.*, 2017; Peredo *et al.*, 2017), with obvious ecological and morphological consequences for early chaeomysticete bulk filtration. Study of two fossils from 27–25 Mya, *Waharoa* (Boessenecker & Fordyce, 2015) and *Horopeta* (Tsai & Fordyce, 2015), suggests the first chaeomysticetes, and crown mysticetes, were either skim or lunge feeders, respectively. More recently, Tsai & Fordyce (2018) concluded the earliest filter-feeding mysticetes were generalists, not specialized filter feeders. Whether continuous or intermittent filterers, it is unlikely, based on fossil rostra and jaws, that they exhibited specialized anatomy (Table 3) such as balaenid-style arched jaws with long plates or a rorqual-like expansive throat pouch with ventral grooves. Nonetheless, given their L_B of about 4.5 m, we calculate A_F from our data-generated equations (Table 1) of 14.31 m^2 for a 'rorqual'-type or a filter with four times greater surface area (58.65 m^2) for a balaenid-type feeder. [Fordyce & Marx (2018) argue the larger *Llanocetus*, as well as aetiocetids and mammalodontids, had no filter.] Although skeletons are incomplete, fossils from all 15 known cetothere genera indicate L_B < 5 m (Gol'din & Startsev, 2017). The L_B of basal eomysticetids is likewise estimated at 4–5 m. At this body size, small relative to extant mysticetes, even high-area filters of continuous ram feeders would not incur the tremendous drag forces experienced by large right and bowhead whales. Many unknowns (such as cetothere or eomysticetid swim speed and prey preference) remain, so we cannot determine with certainty the filtration strategy of original chaeomysticetes.

Curiously, although our simplest (2D) model shows convergence of balaenid- and 'rorqual'-style filters at L_B = 4.68 m (Fig. 2), these trajectories show no convergence in our 3D/3D+ models (Figs 3, 4). This may have non-trivial implications for the evolution of the earliest (proto-)baleen, before the disparate filtration strategies evolved. Although speculative, baleen of the first filtering mysticetes was probably tooth-like in form and perhaps size, with plate width similar to thickness and large inter-plate gaps. This filter architecture is primarily 2D, with little surface area. The 3D models emphasize complex baleen geometry, with mediolaterally wider (chord-wise), blade-like plates that the earliest baleen may not have exhibited. We contend that complex baleen filters arose later in crown mysticetes.

Both intermittent and continuous filtration alternatives are plausible for the first edentulous mysticetes, but some type of intermittent filtration – surely with smaller intraoral volumes than the expansive lunges of rorquals (perhaps more like grey whales) – was probably the initial feeding mode for at least two reasons. First, intermittent filtration depends on discrete, raptorial-style prey collection, which is logically less derived from the ancestral condition.

Second, intermittent filtration requires a relatively smaller filter. The small dimensions of the earliest fossilized baleen (with plates perhaps 10–15 cm long and about 50 plates per rack; Gioncada *et al.*, 2016; Marx *et al.*, 2017) support this contention, as does the lack of rostral arching to accommodate tall racks. Even if as noted above balaenids are phylogenetically more basal than rorquals, the much larger A_F needed for continuous ram filtration is probably a specialized derivation – as is, in truth, the highly derived suction or lunge-feeding of extant intermittent filterers. Nonetheless, continuous filtration, as employed by large sharks, rays and (extinct) bony fishes (Motta *et al.*, 2010; Paig-Tran *et al.*, 2013) of 4–5 m body size similar to that of basal mysticetes, is an intriguing pattern. Continuous filterers need separate orifices for unidirectional incurrent/excurrent flow (Paig-Tran *et al.*, 2013; Potvin & Werth, 2017). Although balaenid outflow does not involve the pharynx as it does in fishes (Werth, 2004), balaenids nonetheless feed for long periods (up to 10 min) before swallowing accumulated prey (Werth, 2001). This ability to subsist on smaller, less energy-rich prey than that of rorquals puts balaenids in a niche similar to that of basking and whale sharks and manta rays. Although intermittently feeding rorquals take large, elusive prey, they do so with considerable expenditure of energy due to the high demands of locomotion and engulfment. Clearly these strategies represent divergent guilds, with sei whales occupying an intermediate position and pygmy right whales perhaps also bridging the gap due to their small body (L_B) and baleen filter size (A_F) at the continuous/intermittent filtration convergence point.

ACKNOWLEDGMENTS

We thank several individuals and institutions for providing access to baleen specimens, including Charley Potter of the Smithsonian Institution's NMNH; Bill McClellan and Erin Fougeres of the NMFS Marine Mammal Stranding Network; Tom Pitchford of the Florida Fish and Wildlife Conservation Commission; J. Craig George and Todd Sformo of Alaska's North Slope Borough Department of Wildlife Management and captains of the Alaska Eskimo Whaling Commission; Kristján Loftsson and the staff of Hvalur H/F; Scott Kraus of the New England Aquarium; Charles Mayo of the Provincetown Center for Coastal Studies; Steven van der Mije and Guido Keijl of the Naturalis Biodiversity Center; Chris Conroy of Berkeley's Museum of Vertebrate Zoology; Judy Chupasko of Harvard's Museum of Comparative Zoology; and Chris Stinson of the Beaty Biodiversity Museum. We thank Nick Pyenson, Brian Kot, Roger Payne, Tom Ford, Peter van de Graaf and Peter Madsen for discussion of the ideas presented here. C-H. Tsai and an anonymous reviewer provided useful comments. JP was supported by NSF Integrative Organismal System grant 1656656. JAG and DEC were supported by the Office of Naval Research's Young Investigator Program, National Science Foundation Integrative Organismal Systems grant 1656691, and a Stanford University Terman Fellowship. RES was supported by Natural Sciences and Engineering Research Council of Canada grant RGPIN 312039-13.

AUTHOR CONTRIBUTIONS

JAG and AJW conceived the study; all authors designed the project, supplying ideas and evidence. AJW conducted the morphometric analysis with help from MMJ and JP. JP ran the mathematical model; JAG and DEC collected and analysed tag data. AJW wrote the paper and prepared figures. All authors assisted with editing and approved the final version.

DATA ACCESSIBILITY

All data are available in online supplements.

REFERENCES

Ahlborn BK, Blake RW, Chan KHS. 2009. Optimal fineness ratio for minimum drag in large whales. *Canadian Journal of Zoology* **87:** 124–131.

Alexander RM. 1998. All-time giants: the largest animals and their problems. *Palaeontology* **41:** 1231–1245.

Berta A, Lanzetti A, Ekdale EG, Deméré TA. 2016. From teeth to baleen and raptorial to bulk filter feeding in mysticete cetaceans: the role of paleontological, genetic, and geochemical data in feeding evolution and ecology. *Integrative and Comparative Biology* **56:** 1271–1284.

Blevins RD. 1984. *Applied fluid dynamics handbook*. New York: Van Nostrand Reinhold.

Boessenecker RW, Fordyce RE. 2015. Anatomy, feeding ecology, and ontogeny of a transitional baleen whale: a new genus and species of Eomysticetidae (Mammalia: Cetacea) from the Oligocene of New Zealand. *PeerJ* **3:** 1129.

Brainerd EL. 2001. Caught in the crossflow. *Nature* **412:** 387–388.

Brodie P, Vikingsson G. 2009. On the feeding mechanisms of the sei whale (*Balaenoptera borealis*). *Journal of Northwest Atlantic Fisheries Science* **42:** 49–54.

Cade DE, Friedlaender AS, Calambokidis J, Goldbogen JA. 2016. Kinematic diversity in rorqual whale feeding mechanisms. *Current Biology* **26:** 2617–2624.

Deméré TA, McGowen MR, Berta A, Gatesy J. 2008. Morphological and molecular evidence for a stepwise evolutionary transition from teeth to baleen in mysticete whales. *Systematic Biology* **57:** 15–37.

Fitzgerald EMG. 2010. The morphology and systematics of *Mammalodon colliveri*, a toothed mysticete from the Oligocene of Australia. *Zoological Journal of the Linnean Society* **158:** 367–476.

Fordyce RE, Marx FG. 2013. The pygmy right whale *Caperea marginata*: the last of the cetotheres. *Proceedings of the Royal Society B: Biological Sciences* **280:** 2645.

Fordyce RE, Marx FG. 2018. Gigantism precedes filter feeding in baleen whale evolution. *Current Biology* **28:** 1–7.

Friedlaender AS, Goldbogen JA, Nowacek DP, Read AJ, Johnston D, Gales N. 2014. Feeding rates and under-ice foraging strategies of the smallest lunge filter feeder, the Antarctic minke whale (*Balaenoptera bonaerensis*). *Journal of Experimental Biology* **217:** 2851–2854.

Fortune SME, Trites AW, Perryman WL, Moore MJ, Pettis HM, Lynn MS. 2012. Growth and rapid early development of North Atlantic right whales (*Eubalaena glacialis*). *Journal of Mammalogy* **93:** 1342–1354.

Fox RW, McDonald AT. 1978. *Introduction to fluid mechanics, 2nd edn*. New York: Wiley.

Gatesy J, Geisler JH, Chang J, Buell C, Berta A, Meredith RW, Springer MS, McGowen MR. 2013. A phylogenetic blueprint for a modern whale. *Molecular Phylogenetics and Evolution* **66:** 479–506.

Geisler JH, Boessenecker RW, Brown M, Beatty BL. 2017. The origin of filter feeding in whales. *Current Biology* **2017:** 2036–2042.

George JC, Bockstoce JR, Punt AE, Botkin DB. 2007. Preliminary estimates of bowhead whale body mass and length from Yankee commercial oil yield records. *Report to 59th International Whaling Commission SC59/BRG5*: 1–11.

George JC, Stimmelmayr R, Suydam R, Usip S, Givens G, Sformo T. Thewissen JGM. 2016. Severe bone loss as part of the life history strategy of bowhead whales. *PLoS ONE* **11:** e0156753.

Gioncada A, Collareta A, Gariboldi K, Lambert O, DiCelma C, Bonaccorsi E, Urbina M, Bianucci G. 2016. Inside baleen: exceptional microstructure preservation in a late Miocene whale skeleton from Peru. *Geology* **44:** 839–842.

Goldbogen JA, Cade D, Calambokidis J, Friedlaender AS, Potvin J, Segre PS, Werth AJ. 2017. How baleen whales feed: the biomechanics of engulfment and filtration. *Annual Reviews of Marine Science* **9:** 367–386.

Goldbogen JA, Calambokidis J, Croll D, McKenna MF, Potvin J, Pyenson ND, Schoor G, Shadwick RE, Tershy BR. 2012a. Scaling of lunge feeding performance in rorqual whales: mass-specific energy expenditure increases with body size and progressively limits diving capacity. *Functional Ecology* **26:** 216–226.

Goldbogen JA, Calambokidis J, Friedlaender AS, Francis J, DeRuiter SL, Stimpert AK, Falcone E, Southall BL. 2012b. Underwater acrobatics by the world's largest predator: 360 degrees rolling manoeuvres by lunge-feeding blue whales. *Biology Letters* **9: 0986.**

Goldbogen JA, Calambokidis J, Oleson E, Potvin J, Pyenson ND, Schorr G, Shadwick RE. 2011. Mechanics, hydrodynamics and energetics of blue whale lunge feeding: efficiency dependence on krill density. *Journal of Experimental Biology* **214:** 131–146.

Goldbogen JA, Calambokidis J, Shadwick RE, Oleson E, McDonald MA, Hildebrand JA. 2006. Kinematics of foraging dives and lunge-feeding in fin whales. *Journal of Experimental Biology* **209:** 1231–1244.

Goldbogen JA, Friedlaender AS, Calambokidis J, McKenna MF, Simon M, Nowacek DP. 2013. Integrative approaches to the study of baleen whale diving behavior, feeding performance, and foraging ecology. *Bioscience* **63:** 90–100.

Goldbogen JA, Hazen EL, Friedlaender AS, Calambokidis J, DeRuiters SL, Stimpert AK, Southall BL. 2015. Prey density and distribution drive the three-dimensional foraging strategies of the largest filter feeder. *Functional Ecology* **29:** 951–961.

Goldbogen JA, Madsen PT. 2018. The evolution of foraging capacity and gigantism in cetaceans. *Journal of Experimental Biology* **221: doi:** 10.1242/jeb.166033.

Goldbogen JA, Potvin J, Shadwick RE. 2010. Skull and buccal cavity allometry increase mass-specific engulfment capacity in fin whales. *Proceedings of the Royal Society B: Biological Sciences* **277:** 861–868

Gol'din P, Startsev D. 2017. A systematic review of cetotherе baleen whales (Cetacea, Cetotheriidae) from the Late Miocene of Crimea and Caucasus, with a new genus. *Papers in Palaeontology* **3:** 49–68.

Hazen EL, Friedlaender AS, Thompson MA, Ware C, Weinrich MT, Halpin PN, Wiley DN. 2009. Fine-scale prey aggregations and foraging ecology of humpback whales (*Megaptera novaeangliae*). *Marine Ecology Progress Series* **395:** 75–89.

Hocking DP, Marx FG, Fitzgerald EMG, Evans AR. 2017. Ancient whales did not filter feed with their teeth. *Biology Letters* **13:** 20170348.

Horwood J. 2017. Sei whale. In: Wursig B, Thewissen JGM, Kovacs, KN, eds. *Encyclopedia of marine mammals*. San Diego: Academic Press, 845–847.

Ishii M, Murase H, Fukuda Y, Sawada K, Sasakura T, Tamura T, Bando T, Matsuoka K, Shinohara A, Nakatsuka S, Katsumata N, Okazaki M, Miyashita K, Mitani Y. 2017. Diving behavior of sei whales *Balaenoptera borealis* relative to the vertical distribution of their potential prey. *Mammal Study* **42:** 191–199.

Jensen MM, Saladrigas AH, Goldbogen JA. 2017. Comparative three-dimensional morphology of baleen: cross-sectional profiles and volume measurements using CT images. *The Anatomical Record* **300:** 1942–1952.

Kawamura A. 1974. Food and feeding ecology in the southern sei whale. *Scientific Reports of the Whales Research Institute* **26:** 25–144.

Kawamura A. 1980. A review of food of balaenopterid whales. *Scientific Reports of the Whales Research Institute* **32:** 155–198.

Kemper CM. 2017. Pygmy right whale. In: Wursig B, Thewissen JGM, Kovacs KM, eds. *Encyclopedia of marine mammals, 3rd edn*. San Diego: Academic Press, 790–792.

Kulmov SK. 1966. Plankton and the feeding of the whalebone whales (Mystacoceti). *Trudy Instituta Okeanologii* **51:** 142–156.

Lambert O, Martínez-Cáceres M, Bianucci G, DiCelma C, Salas-Gismondi R, Steurbaut E, Urbina M, de Muizon C. 2017. Earliest mysticete from the Late Eocene of Peru sheds new light on the origin of baleen whales. *Current Biology* **27:** 1535–1541.

Lambertsen RH. 1983. Internal mechanism of rorqual feeding. *Journal of Mammalogy* **64:** 76–88.

Lambertsen RH, Hintz RJ, Lancaster WC, Hirons A, Kreiton KJ, Moor C. 1989. Characterization of the functional morphology of the mouth of the bowhead whale, *Balaena mysticetus*, with special emphasis on the feeding and filtration mechanisms. *Report to the Department of Wildlife Management*. Barrow: North Slope Borough.

Lauder GV. 1985. Aquatic feeding in lower vertebrates. In: Hildebrand M, Bramble DM, Liem KF, Wake DB, eds. *Functional vertebrate morphology*. Cambridge: Harvard University Press, 210–229.

Leaper R, Lavigne D. 2007. How much do large whales eat? *Journal of Cetacean Resource Management* **9:** 179–188.

Lockyer C. 1976. Body weight of some species of large whales. *ICES Journal of Marine Science* **36:** 259–273.

Marx FG, Collareta A, Gioncada A, Post K, Lambert O, Bonaccorsi E, Urbina M, Bianucci G. 2017. How whales used to filter: exceptionally preserved baleen in a Miocene cetotheriid. *Journal of Anatomy* **231:** 212–220.

Marx FG, Fordyce RE. 2015. Baleen boom and bust: a synthesis of mysticete phylogeny, diversity and disparity. *Royal Society Open Science* **2:** 1–14.

Marx FG, Fordyce RE. 2016. A link no longer missing: new evidence for the cetotheriid affinities of *Caperea*. *PLoS One* **11:** 0164059.

Marx FG, Hocking DP, Park T, Ziegler T, Evans AR, Fitzgerald EMG. 2016. Suction feeding preceded filtering in baleen whale evolution. *Memoirs of Museum Victoria* **75:** 71–82.

Mayo CA, Letcher BH, Scott S. 2001. Zooplankton filtering efficiency of the baleen of a North Atlantic right whale, *Eubalaena glacialis*. *Journal of Cetacean Resource Management* **2:** 225–229.

McCurry MR, Fitzgerald EMG, Evans AR, Adams JW, McHenry CR. 2017. Skull shape reflects prey size niche in toothed whales. *Biological Journal of the Linnean Society* **121:** 936–946.

Michaud J, Taggart CT. 2007. Lipid and gross energy content of North Atlantic right whale food, *Calanus finmarchicus*, in the Bay of Fundy. *Endangered Species Research* **2007:** 77–94.

Motta PJ, Maslanka M, Hueter RE, Davis RL, de la Parra R, Mulvany SL, Habegger ML, Strother JA, Mara KR, Gardiner JM, Tyminski JP, Zeigler LD. 2010. Feeding anatomy, filter-feeding rate, and diet of whale sharks *Rhincodon typus* during surface ram filter feeding off the Yucatan Peninsula, Mexico. *Zoology* **113:** 199–212.

Nemoto T. 1959. Food of baleen whales with reference to whale movements. *Scientific Reports of the Whales Research Institute* **14:** 149–241.

Nemoto T. 1970. Feeding pattern of baleen whales in the ocean. In: Steele, JH, ed. *Marine food chains*. Edinburgh: Oliver and Boyd, 241–252.

Nikaido M, Hamilton H, Makino H, Sasaki T, Takahashi K, Goto M, Kanda N, Pastene LA, Okada N. 2006. Baleen whale phylogeny and a past extensive radiation event revealed by SINE insertion analysis. *Molecular Biology and Evolution* **23:** 866–873.

Nishiwaki M. 1950. On the body weight of whales. *Scientific Reports of the Whales Research Institute* **4:** 184–209.

Olsen E, Budgell P, Head E, Kleivane L, Nøttestad L, Prieto R, Silva MA, Skov H, Vikingsson GA, Waring G, Øien N. 2009. First satellite-tracked long distance movement of a sei whale (*Balaenoptera borealis*) in the North Atlantic. *Aquatic Mammals* **35:** 313–318.

Packard GC. 2013. Is logarithmic transformation necessary in allometry? *Biological Journal of the Linnean Society* **109:** 476–486.

Packard GC. 2017. The essential role for graphs in allometric analysis. *Biological Journal of the Linnean Society* **120:** 468–473.

Paig-Tran E, Kleinteich T, Summers AP. 2013. Filter pads and filtration mechanisms of the devil rays: variation at macro and microscopic scales. *Journal of Morphology* **274:** 1026–1043.

Peredo CM, Pyenson ND, Boersma AT. 2017. Decoupling tooth loss from the evolution of baleen in whales. *Frontiers in Marine Science* **4:** 1–11.

Pivorunas A. 1976. A mathematical consideration of the function of baleen plates and their fringes. *Scientific Reports of the Whales Research Institute* **28:** 37–55.

Pivorunas A. 1979. The feeding mechanisms of baleen whales. *American Scientist* **67:** 432–440.

Potvin J, Goldbogen JA, Shadwick RE. 2009. Passive versus active engulfment: verdict from trajectory simulations of lunge-feeding fin whales *Balaenoptera physalus*. *Journal of the Royal Society Interface* **6:** 1005–1025.

Potvin J, Goldbogen JA, Shadwick RE. 2012. Metabolic expenditures of lunge feeding rorquals across scale: implications for the evolution of filter feeding and the limits to maximum body size. *PLoS One* **7:** 44854.

Potvin J, Werth AJ. 2017. Oral cavity hydrodynamics and drag production in balaenid whale suspension feeding. *PLoS One* **12:** 5220.

Pyenson ND. 2017. The ecological rise of whales chronicled by the fossil record. *Current Biology* **27:** 558–564.

Pyenson ND, Vermeij GJ. 2016. The rise of ocean giants: maximum body size in Cenozoic marine mammals as an indicator for productivity in the Pacific and Atlantic Oceans. *Biology Letters* **12:** 20160186.

Riesch R, Barrett-Lennard LG, Ellis GM, Ford JKB, Deecke VB. 2012. Cultural traditions and the evolution of reproductive isolation: ecological speciation in killer whales? *Biological Journal of the Linnean Society* **106:** 1–17.

Sanderson SL, Wassersug RL. 1990. Suspension-feeding vertebrates. *Scientific American* **262:** 96–101.

Schultz LP. 1938. Can the weight of whales and large fish be calculated? *Journal of Mammalogy* **19:** 480–487.

Sekiguchi K, Best PB, Kaczmaruk BZ. 1992. New information on the feeding habits and baleen morphology of the pygmy right whale *Caperea marginata*. *Marine Mammal Science* **8:** 288–293.

Shadwick RE, Goldbogen JA, Potvin J, Pyenson ND, Vogl AW. 2013. Novel muscle and connective tissue design enables high extensibility and controls engulfment volume in lunge-feeding rorqual whales. *Journal of Experimental Biology* **216:** 2691–2701.

Simon M, Johnson M, Tyack P, Madsen PT. 2009. Behaviour and kinematics of ram filtration in bowhead

whales (*Balaena mysticetus*). *Proceedings of the Royal Society B* **276:** 3819–3828.

Simon M, Johnson M, Madsen PT. 2012. Keeping momentum with a mouthful of water: behavior and kinematics of humpback whale lunge feeding. *Journal of Experimental Biology* **215:** 3786–3798.

Slater GJ, Goldbogen JA, Pyenson ND. 2017. Independent evolution of baleen whale gigantism linked to Plio-Pleistocene ocean dynamics. *Proceedings of the Royal Society B* **284:** 20170546.

Szewciw LJ, de Kerkhove DG, Grime GW, Fudge DS. 2010. Calcification provides mechanical reinforcement to whale baleen alpha keratin. *Proceedings of the Royal Society B* **277:** 2597–2605.

Thewissen JGM, Hieronymus TL, George JC, Suydam R, Stimmelmayr R, McBurney D. 2017. Evolutionary aspects of the development of teeth and baleen in the bowhead whale. *Journal of Anatomy* **230:** 549–566.

Tomilin AG. 1954. Adaptive types of the Order Cetacea. *Zoologicheskii Zhurnal* **33:** 677–691.

Tsai C-H, Fordyce RE. 2014a. Disparate heterochronic processes in baleen whale evolution. *Evolutionary Biology* **41:** 299–307.

Tsai C-H, Fordyce RE. 2014b. Juvenile morphology in baleen whale phylogeny. *Naturwissenschaften* **101:** 765–769.

Tsai C-H, Fordyce RE. 2015. The earliest gulp-feeding mysticete from the Oligocene of New Zealand. *Journal of Mammalian Evolution* **22:** 535–560.

Tsai C-H, Fordyce RE. 2018. A new archaic baleen whale *Toipahautea waitaki* (early Late Oligocene) and the origins of crown Mysticeti. *Royal Society Open Science* **5:** 172453.

Werth AJ. 2000. Marine mammals. In: Schwenk K, ed. *Feeding: form, function, and evolution in tetrapod vertebrates*. New York: Academic Press, 475–514.

Werth AJ. 2001. How do mysticetes remove prey trapped in baleen? *Bulletin of the Museum of Comparative Zoology* **156:** 189–203.

Werth AJ. 2004. Models of hydrodynamic flow in the bowhead whale filter feeding apparatus. *Journal of Experimental Biology* **207:** 3569–3580.

Werth AJ. 2012. Hydrodynamic and sensory factors governing response of copepods to simulated predation by baleen whales. *International Journal of Ecology* **2012:** 208913.

Werth AJ. 2013. Flow-dependent porosity and other biomechanical properties of mysticete baleen. *Journal of Experimental Biology* **216:** 1152–1159.

Werth AJ, Harriss RW, Rosario MV, George JC, Sformo TL. 2016a. Hydration affects the physical and mechanical properties of baleen tissue. *Royal Society Open Science* **3:** 160591.

Werth AJ, Ito H. 2017. Sling, scoop, squirter: anatomical features facilitating prey transport, concentration, and swallowing in rorqual whales (Mammalia: Mysticeti). *The Anatomical Record* **300:** 2070–2086.

Werth AJ, Potvin J. 2016. Baleen hydrodynamics and morphology of cross-flow filtration in balaenid whale suspension feeding. *PLoS ONE* **11:** e0150106.

Werth AJ, Straley JM, Shadwick RE. 2016b. Baleen wear reveals intraoral water flow patterns of mysticete filter feeding. *Journal of Morphology* **277:** 453–471.

Williamson GR. 1973. Counting and measuring baleen and ventral grooves of whales. *Scientific Reports of the Whales Research Institute* **24:** 279–292.

Young S. 2012. *The comparative anatomy of baleen: evolutionary and ecological implications*. Unpublished MSc thesi, San Diego State University.

Young S, Deméré TE, Ekdale EG, Berta A, Zellmer N. 2015. Morphometrics and structure of complete baleen racks in gray whales (*Eschrichtius robustus*) from the Eastern North Pacific Ocean. *Anatomical Record* **298:** 703–719.